Realization of an All-Solid-State Cryocooler Using Optical Refrigeration

Junwei Meng*[a], Alexander R. Albrecht[a], Aram Gragossian[a], Eric Lee[a], Azzurra Volpi[a], Mohammadreza Ghasemkhani[a], Markus P. Hehlen[b], Richard I. Epstein[c], Mansoor Sheik-Bahae[a]

[a]University of New Mexico, Dept. of Physics and Astronomy, 1919 Lomas Blvd. NE, Albuquerque, NM 87131, USA;

[b]Los Alamos National Laboratory, Engineered Materials (MST-7), Mailstop E546, Los Alamos, NM 87545, USA;

[c]ThermoDynamic Films LLC, Santa Fe, NM 87505, USA.

ABSTRACT

Optical refrigeration of rare-earth-doped solids has reached the boiling point of argon, 87 K, and is expected to cool to that of nitrogen, 77 K, in the near future. This technology is poised to pave the way to compact, reliable, and vibration-free all-solid-state optical cryocoolers. By attaching the Yb:YLF cooling crystal to a cold finger via a double 90° kink thermal link, we have cooled a silicon temperature sensor to below 151 K. An advanced design of the thermal link and the clamshell surrounding the cooled assembly successfully controlled the flow of heat and radiation to allow cooling of a payload to cryogenic temperatures. Key elements of the design were a low-absorption thermal link material, an optimized thermal link geometry, and a spectrally-selective coating of the clamshell.

Keywords: Optical refrigeration, cryocooler, thermal link, Yb:YLF crystal, rare-earth-doped solids, all-solid-state optical cryocooler.

1. INTRODUCTION

Optical refrigeration in solids was first demonstrated by Epstein *et al* in 1995[1] with Yb^{3+}-doped ZBLANP (Yb:ZBLANP) glass. Since then the field has witnessed tremendous progress on multiple fronts[2–5]. In the early years, the research was focused on Yb:ZBLANP due to the availability of high-purity fluoride glasses. However, owing to the inhomogeneous broadening of Yb^{3+} electronic transitions in glasses and the doping level limited to 4 mol%, optical cooling in these materials could not achieve temperatures below 200 K. The use of crystalline host materials having smaller inhomogeneous broadening has enabled notable improvements in cooling performance, reaching the cryogenic regime[6], and most recently cooling to 87 K has been attained[7]. Improvements in material type and quality, combined with novel optical and thermal management techniques, together with the availability of high-power laser sources at the required wavelength have rendered laser cooling as the only practical all-solid-state, vibration-free cooling technology[2,3,4] that can reach cryogenic temperatures starting from room temperature. This makes optical cryocoolers ideal for applications that are sensitive to vibrations and microphonic noise, such as focal plane arrays, reference cavities for ultra-stable lasers, HgCdTe and germanium sensors, and cryo-electron microscopy[6,8,9].

Solid-state laser cooling is based on anti-Stokes fluorescence, which is the result of the energy exchange between photons and lattice phonons[1, 2, 5, 9, 10, 11]. Low-entropy photons, provided by a narrow-linewidth laser source and having photon energies slightly less than the mean fluorescence energy, are absorbed by an atomic transition. This excitation leaves the system in a non-equilibrium condition. Thermal quasi-equilibrium is subsequently established through the absorption of

*jmeng@unm.edu; www.phys.unm.edu/msbahae/

Tri-Technology Device Refrigeration (TTDR) III, edited by Mansoor Sheik-Bahae, Richard I. Epstein, Bjørn F. Andresen, Tonny Benschop, Joseph P. Heremans, Sergey V. Riabzev, Proc. of SPIE Vol. 10626, 106260B · © 2018 SPIE · CCC code: 0277-786X/18/$18 · doi: 10.1117/12.2305195

lattice phonons, followed by an anti-Stokes radiative decay (fluorescence). The solid cools due to the respective higher-energy and higher-entropy emitted photons that escape the system. For the Yb^{3+} ion, the laser excitation occurs from the top of the $^2F_{7/2}$ ground-state multiplet to the bottom of the $^2F_{5/2}$ excited-state multiplet. In order to achieve net cooling, and further cool the crystal to low temperatures, a very high external quantum efficiency (η_{ext}) as well as extremely low impurity concentrations are required. The cooling efficiency (η_c) is defined as the ratio of the cooling power, P_{cool}, and the absorbed power, P_{abs}, and it can be written as:[10].

$$\eta_c = \frac{P_{cool}}{P_{abs}} = \eta_{ext}\left[\frac{\alpha_r(\lambda,T)}{\alpha_r(\lambda,T)+\alpha_b}\right]\frac{\lambda}{\lambda_f(T)} - 1 \quad (1)$$

where the term in square brackets represents the absorption efficiency, which quantifies the fraction of pump power absorbed by the resonant transition $\alpha_r(\lambda, T)$ relative to the total absorption by the medium, which also includes parasitic (background) absorption, α_b. Here, λ is the wavelength of the pump laser, and λ_f is the mean fluorescence wavelength exiting the system. Both η_{ext} and α_b are assumed to be independent of temperature.

2. RESULTS AND DISCUSSION

2.1 Characterization of the cooling crystal

Full characterization of the Yb:YLF crystal cooling efficiency requires measurement of the four key parameters $\lambda_f, \alpha_b, \alpha_r,$ and η_{ext}, including their temperature and wavelength dependencies. The quantities α_b and η_{ext} can be evaluated by using a laser calorimetric method, referred to as Laser-Induced Temperature Modulation Spectroscopy (LITMoS)[4]. This method measures the relative temperature changes induced by a tunable laser source (CW Ti:sapphire laser, 940 nm – 1090 nm). The temperature change induced by the incident laser is measured using an uncooled bolometric thermal camera. When normalized to the absorbed laser power, it is proportional to the cooling efficiency for relatively small temperature changes. The absorbed power is computed from the incident laser power using the (temperature dependent) absorption spectrum. The latter is obtained from polarized ($\vec{E} \parallel \vec{c}$ and $\vec{E} \perp \vec{c}$) temperature-dependent (30–300 K) fluorescence spectra $S(\lambda, T)$ by exploiting the concept of reciprocity through the McCumber relation [11],

$$\alpha_r(\lambda, T) \propto \lambda^5 S(\lambda, T) e^{hc/\lambda k_B T} \quad (2)$$

The unpolarized fluorescence spectra are used to calculate the mean fluorescence wavelength $\lambda_f(T)$. The LITMoS test is typically only performed at room temperature. A good 10%Yb:YLF cooling crystal typically yields $\alpha_b \leq 3 \pm 0.5 \times 10^{-4}$ cm^{-1} and $\eta_{ext} = 99.0(\pm 0.1)\%$ [12, 13]. Assuming these values to be temperature independent, Eq. (1) can now be evaluated as function of wavelength and temperature. This is shown in Fig. 1, where blue denotes cooling and red denotes heating. The minimum achievable temperature (MAT) of ≅ 90 K is predicted for a pump laser at λ = 1020 nm, corresponding to the lowest-energy Stark transition between the two multiplets. In the subsequent "power cooling" experiments, we therefore used a custom 1020-nm high-power (50 W) fiber laser to pump the crystal and achieve cooling to low temperatures.

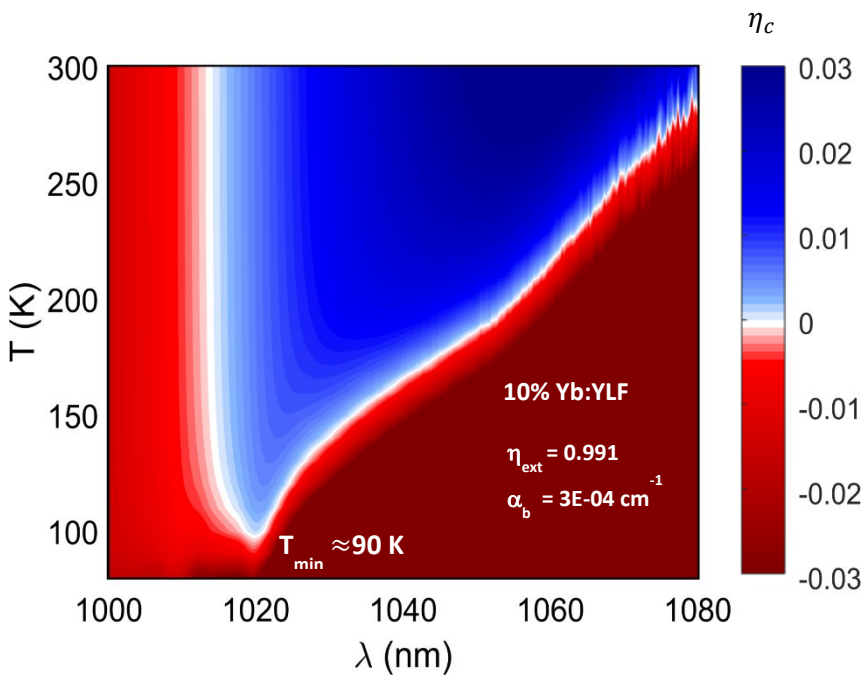

Figure 1. Cooling efficiency $\eta_c(\lambda, T)$ for one of the 10%Yb:YLF crystals. Blue regions show cooling, red regions show heating, and the white line represents the spectrum of the minimum achievable temperature (MAT). The global MAT of 90 K is highlighted. α_b *and* η_{ext} obtained from a room temperature LITMoS test are indicated.

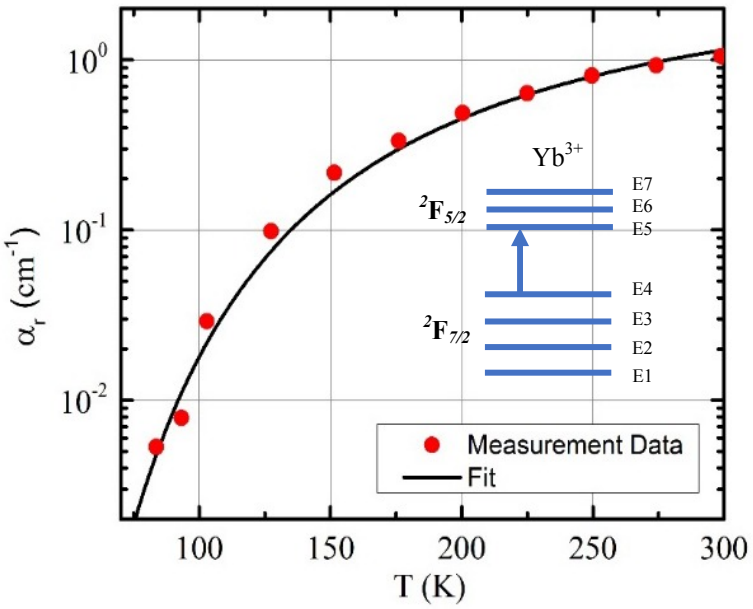

Figure 2. Measured absorption coefficient of 10%Yb:YLF (red dots) at 1020 nm corresponding to the lowest-energy Stark transition $^2F_{7/2}(E4) \rightarrow {}^2F_{5/2}(E5)$ of Yb^{3+}. The solid line is a least-squares fit of the function $\alpha_r(T) = A[1 + \exp(\delta E_g / k_B T)]^{-1}$ to the experimental data. Here, $\delta E_g \sim 460$ cm^{-1} is the width of the $^2F_{7/2}$ ground-state multiplet in this material, and A is a constant.

2.2 Herriot cell

A non-resonant cavity design was used in order to maximize the pump-laser absorption by providing multiple passes of the pump laser through the crystal. Such a multi-pass pump geometry was especially important at lower temperatures, where the Boltzmann population of, and therefore the resonant absorption coefficient from, the highest-energy crystal-field level of the Yb^{3+} ground-state multiplet decreases rapidly with decreasing temperature [7]. The resonant absorption coefficient at 1020 nm as function of temperature is shown in Fig. 2. Non-resonant multi-pass cavities (Herriott cells [7,14]) offer a simple and practical solution to realizing high absorption efficiencies. We used the two implementations shown in Fig. 3. Fig. 3a shows a circular beam path that was formed by one plane mirror with an off-center hole to admit the pump laser to the cavity and a spherical mirror with radius of curvature R=50 cm. Due to the finite hole size and laser beam waist, 20–30 passes of the pump laser through the crystal could typically be achieved. Fig. 3b shows a square beam path geometry with a significantly higher number of passes (up to 500). This geometry used a spherical mirror (R=50 cm) with a hole at the center as an input mirror and a cylindrical mirror (R_x=∞ and R_y=50 cm) as an end mirror. This cavity provided for >90% absorption of the pump laser in the crystal for temperatures down to 100 K.

To minimize the heat load on the crystal, the crystal was placed on top of 4 optical fibers in a vacuum chamber that was evacuated to a pressure of $< 10^{-6}$ Torr in order to minimize conductive and convective heat loads, respectively. In addition, the sample was surrounded by a tightly-fitting clamshell coated with a low-emissivity material (TiNOX from Almeco) and cooled to -10 °C. Using the above mentioned Herriott cell in conjunction with this clamshell geometry has previously allowed us to cool a 10%Yb:YLF crystal to 91 K [4].

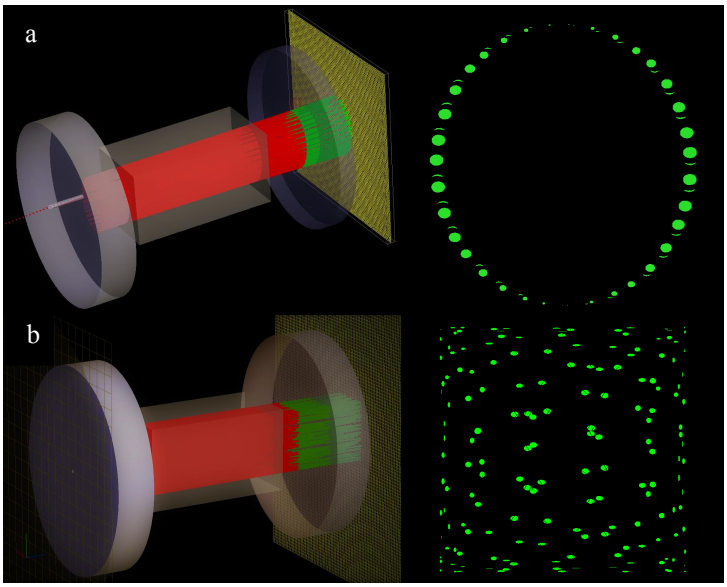

Figure 3. Illustrations of the Herriot cell geometries (left) and associated calculated pump-laser spatial distributions at the back mirror (right) for (a) the circular and (b) the square multi-pass pattern.

2.3 Thermal link and cold-finger

Attaching a payload directly to the Yb:YLF crystal is not practical, as the payload would experience significant heating due to direct exposure to and absorption of the intense crystal fluorescence. Therefore, for practical applications a thermal link is inserted between the cooling crystal and a copper cold-finger to which the payload is attached. An ideal thermal link is designed to reject >99.9% of the fluorescence from reaching the cold-finger, has low absorption to not introduce laser-induced heating itself, and has a high thermal conductivity to minimize the thermal gradient between the cooling crystal and the payload. In the present optical cryocooler, sapphire was used as the thermal link material because of its high thermal conductivity especially at low temperatures (600–800 W $m^{-1}K^{-1}$ at 100 K[15]) and low residual absorption at wavelengths around 1 μm ($\alpha \approx 3 \times 10^{-4} cm^{-1}$ [15]). As shown in Figures 4a and 4b, the present thermal link featured two 90° kinks that helped reject Yb:YLF fluorescence from reaching the cold-finger attached at the other end of the thermal link. The two ends of the thermal link required special attention. The interface of the link with the cold-finger was coated with a silver mirror to reflect any residual transmitted fluorescence, and the link was then attached to the cold-finger using thermal epoxy. The interface of the link with the cooling crystal was bonded with low optical absorption glue. The thermal link and cold-finger geometry used in the present experiment is shown in Fig. 4. One arm of the thermal link surface was textured for effective light extraction as shown in Fig. 7.

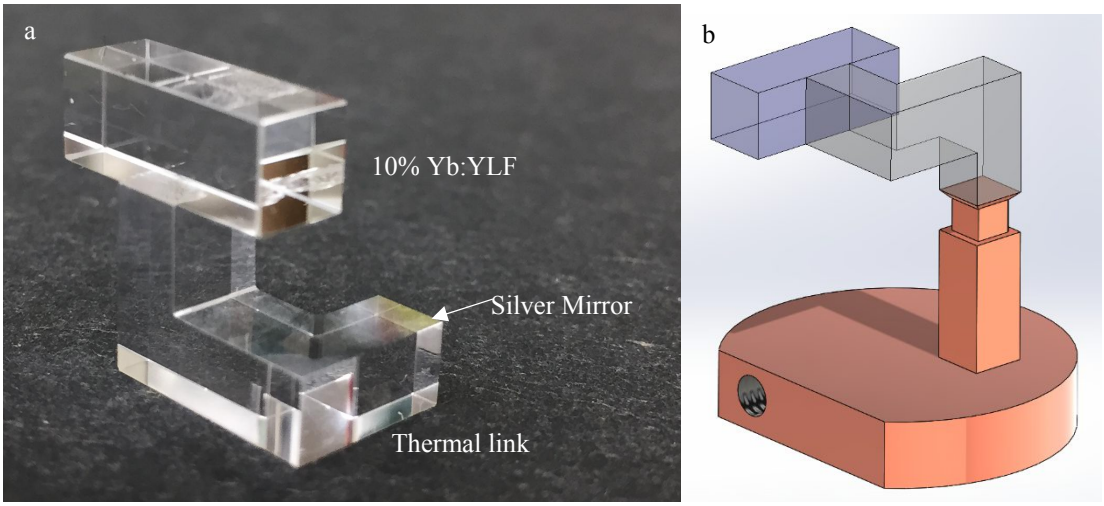

Figure 4. a). The cuboid-shaped 10% Yb:YLF crystal (top) was attached to a double 90° kink sapphire thermal link (bottom) using adhesive, and at the other end, the thermal link was coated with a silver mirror. b). A 3D CAD drawing showing the assembly of cooling crystal, thermal link, and cold-finger.

2.4 Clamshell and laser-cooling assembly

A clamshell structure that closely enveloped and thereby reduced the radiative heat load on the cooled assembly (cooling crystal, thermal link, cold-finger, payload) was implemented. The clamshell absorbs most of the fluorescence emitted by the cooling crystal and therefore must be of high thermal conductivity in order to effectively remove the fluorescence heat load. Geometrically, it should tightly surround the cooled assembly to minimize the radiative heat transfer. The present clamshell was fabricated from copper and internally lined with a high-absorption (near 1 μm) low-emissivity (at thermal wavelengths) coating (TiNOX). Several 5-mm diameter and 5-mm long silica aerogel cylinders were used to support the cold finger inside the clamshell. Silica aerogel is an open-celled mesoporous SiO_2 network having a low mass density of 0.1–0.2 g/cm^3 as well as low optical absorption in the visible and near-infrared spectral range and very low thermal conductivities of ~0.004 W/m·K (at 300 K) and ~0.001 W/m·K (at 100 K) in vacuum[15]. The cold-finger was supported by silica aerogels (blue cylinder components in Fig. 5 and Fig. 6 that allowed for a low conductive heat load from the clamshell to the cold-finger. A Si temperature sensor was attached to the cold-finger as a payload and a means for a direct measurement of the cold-finger temperature. The sensor's electrical leads ran through the vacuum chamber and a vacuum feedthrough to the external data acquisition system.

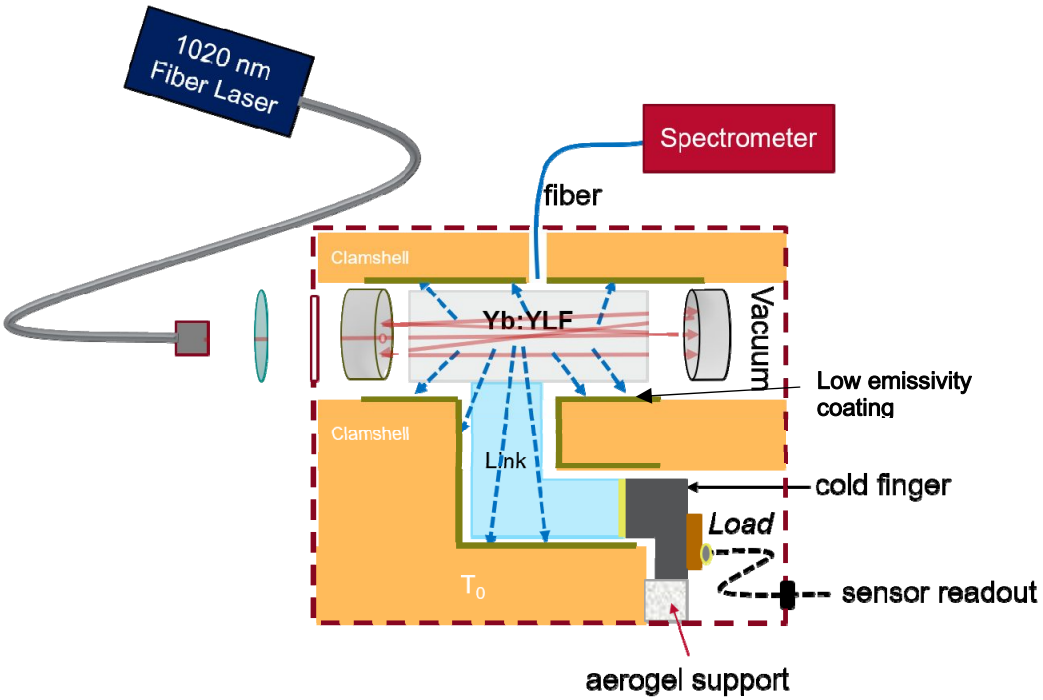

Figure 5. Block diagram (not to scale) showing the components of the optical cryocooler. The laser-cooling material (light gray) was placed inside an astigmatic Herriott cell to provide for multi-pass excitation by the pump laser. The Si temperature sensor payload (yellow-brown) was connected via a cold-finger (gray) and thermal link to the cooling crystal. The clamshell (yellow) surrounded the cooling assembly and was internally coated with TiNOX (yellow-green). The entire system was contained within a vacuum chamber (red). The DLT fiber and spectrometer as well as the pump laser are also shown.

Figure 5 shows a schematic block diagram of the components of the optical cryocooler. The crystal (light gray), thermal link (light blue) and cold-finger (gray) were surrounded by the clamshell (yellow). The Si temperature sensor was attached to the end of the cold-finger. The temperature signal was recorded by using a temperature controller (Lakeshore Cryotronics). The cooling crystal temperature was monitored by using differential luminescence thermometry (DLT) [13]. This technique is based on changes in the shape of the fluorescence spectrum as a function of temperature, and it was implemented by collecting the fluorescence from the crystal with a multimode optical fiber inserted flush with the clamshell wall near the Yb:YLF crystal. The fiber was coupled to a fluorescence spectrometer (Ocean Optics) operating between 600 nm and 1100 nm, which allowed continuous acquisition of spectra. A fiber laser (IPF Photonics) operating at 1020 nm and providing 46 W of output power was used as the pump light source. It was admitted to the vacuum chamber through an AR-coated window and a hole drilled in the incident mirror to allow excitation of the 10%Yb:YLF crystal. The circular-shaped multi-pass Herriott cell geometry (Fig. 3a) was used in the experiment.

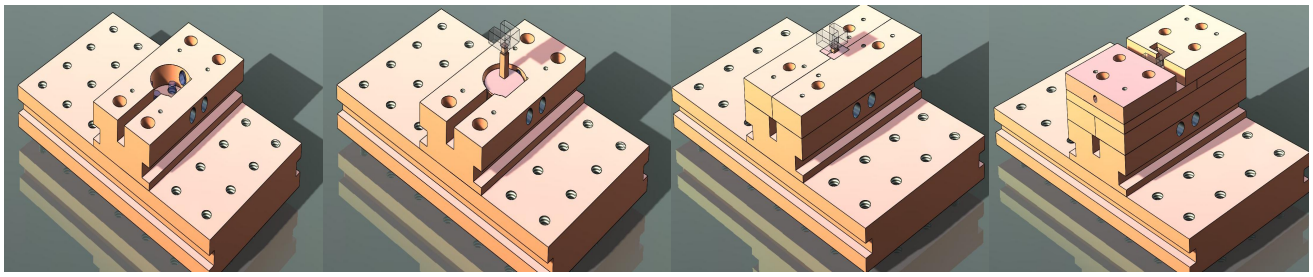

Figure 6. Assembly sequence of the clamshell surrounding the cooled assembly.

Figure 6 shows the assembly sequence of the clamshell. The large copper base plate was liquid cooled (water and propylene glycol mixture) to -10 °C. From left to right, the images show (1) the base layer of the clamshell, with the silica aerogel cylinders (blue) used to support the cold-finger, (2) the cold-finger with the thermal link and crystal inserted on top of the silica aerogel supports, (3) the second clamshell layer surrounding the cold-finger, and (4) the remaining clamshell layers surrounding the cooling crystal. A photograph of the final set up is shown in Fig. 7.

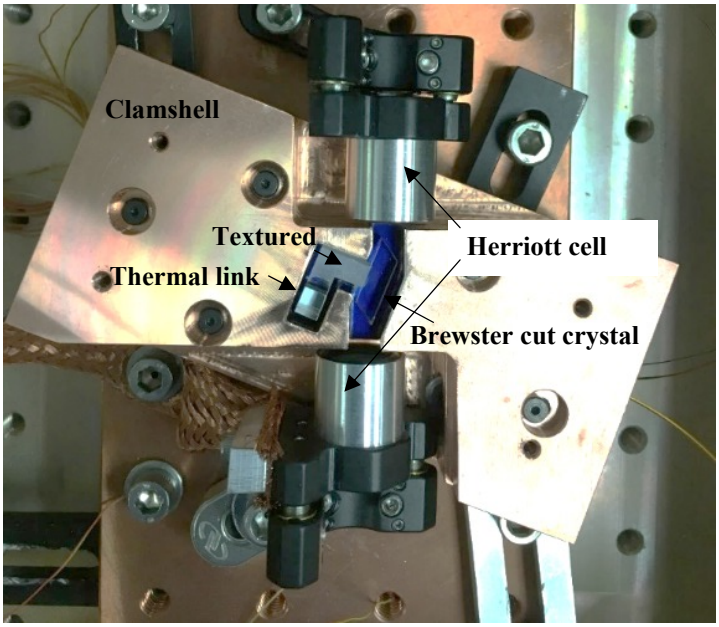

Figure 7. Fully assembled cryocooler with the clamshell's top layer removed to show the Brewster-cut Yb:YLF crystal and the two Herriott cell mirrors. The clamshell was mounted on a water-cooled base held at -10 °C. The entire assembly is placed inside a vacuum chamber.

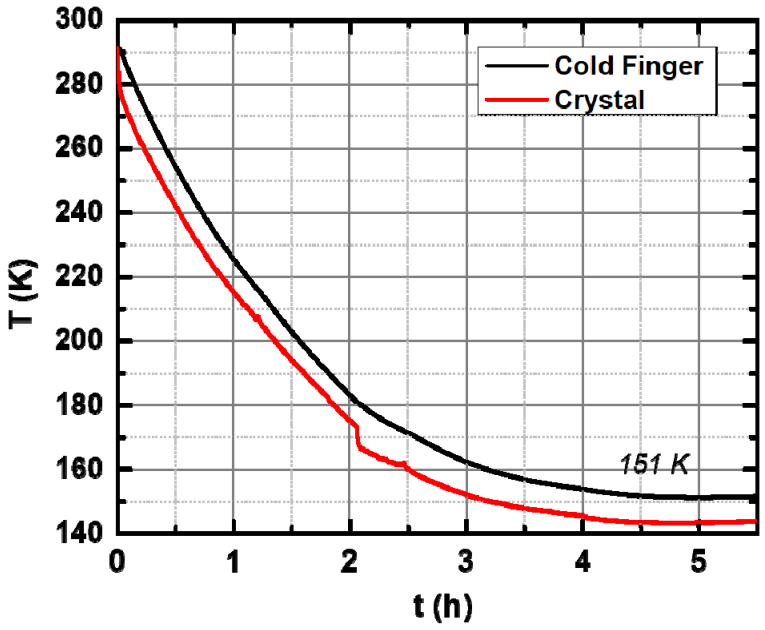

Figure 8. The temperatures of the Si sensor payload (black) and the 10%Yb:YLF crystal (red) are shown as a function of time after turning on the 46 W 1020 nm pump laser.

2.5 Cooling the payload

Figure 8 shows the Si sensor temperature (black) and Yb:YLF crystal temperature derived from DLT (red) as a function of time after turning on the pump laser. The Herriot cell was aligned for 20 pump-laser passes in this experiment. The payload temperature reached 151 K after 5 hours. This, along with a concurrent experiment using an undoped YLF thermal link[16], are the first demonstrations of cooling a realistic load (Si temperature sensor) to the cryogenic regime using optical refrigeration. These data experimentally confirm the effectiveness of the geometry and material choices for the thermal link, cold-finger, aerogel supports, and clamshell discussed above. Note in Fig. 8 that after about two hours, the temperature difference between crystal and payload suddenly increased. This is attributed to delamination of the glue between the thermal link and the cooling crystal as a result of the thermal expansion mismatch between Yb:YLF and sapphire. While stronger adhesives or even adhesive-free bonding[12] could be utilized, a stronger bond may fracture the Yb:YLF crystal, which is softer than sapphire. Another solution is to use an undoped YLF crystal as thermal link material to achieve a close thermal expansion match with the Yb:YLF cooling crystal[16].

3. CONCLUSIONS

We have used an all-solid-state optical refrigerator to cool a Si temperature sensor (payload) to 151 K. This opens the opportunity to using this technology for different applications, which may benefit from this compact, vibration-free cryogenic refrigerator. The all-solid-state optical refrigerator was enabled by several key ingredients: (1) a thermal link and cold-finger allowed for cooling of an arbitrary load, (2) aerogel cylinders to support the cold finger in a mechanically-stable and easily-adjustable manner with minimal thermal conductivity, and (3) a high thermal conductivity clamshell that reduced the radiative load on the system while assisting with the optical isolation of the payload. Future work will focus on a new thermal link design to minimize the thermal expansion mismatch and to improve the thermal conductivity and fluorescence rejection.

ACKNOWLEDGMENTS

The authors acknowledge the support by Air Force Office of Scientific Research (AFOSR) under award numbers FA9550-15-1-024, FA9550-16-1-0362 (MURI), and DARPA STTR program. We thank T. Williamson and K. Baldwin (Los Alamos National Laboratory) for depositing the Ag/Au mirror, and Bernardo Farfan and Guy Symonds from ThermoDynamic Films LLC for useful discussions.

REFERENCES

[1] Epstein, R. I., Buchwald, M. I., Edwards, B. C., Gosnell, T. R. and Mungan, C. E., "Observation of laser-induced fluorescent cooling of a solid," Nature **377**(6549), 500–503 (1995).

[2] Hoyt, C. W., "Laser Cooling in Thulium-doped Solids," Diss. Univ. New Mex., 138 (2003).

[3] Hehlen, M. P., Sheik-Bahae, M. and Epstein, R. I., "Solid-state optical refrigeration," Handb. Phys. Chem. Rare Earths **45**(505), 179–260 (2014).

[4] Melgaard, S. D., Albrecht, A. R., Hehlen, M. P. and Sheik-Bahae, M., "Solid-state optical refrigeration to sub-100 Kelvin regime," Sci. Rep. **6**, 2–7 (2016).

[5] Hehlen, M. P., Sheik-Bahae, M., Epstein, R. I., Melgaard, S. D. and Seletskiy, D. V., "Materials for Optical Cryocoolers," J. Mater. Chem. C **1**(45), 7471 (2013).

[6] Seletskiy, D. V., Melgaard, S. D., Bigotta, S., Di Lieto, A., Tonelli, M. and Sheik-Bahae, M., "Laser cooling of solids to cryogenic temperatures," Nat. Photonics **4**(3), 161–164 (2010).

[7] Gragossian, A., Meng, J., Ghasemkhani, M., Albrecht, A. R. and Sheik-Bahae, M., "Astigmatic Herriott cell for optical refrigeration," Opt. Eng. **56**(1), 11110 (2016).

[8] Seletskiy, D. V., Hehlen, M. P., Epstein, R. I. and Sheik-Bahae, M., "Cryogenic optical refrigeration," Adv. Opt. Photonics **4**(1), 78 (2012).

[9] Melgaard, S., Seletskiy, D., Polyak, V., Asmerom, Y. and Sheik-Bahae, M., "Identification of parasitic losses in Yb:YLF and prospects for optical refrigeration down to 80K," Opt. Express **22**(7), 7756 (2014).

[10] Sheik-Bahae, M. and Epstein, R. I., "Optical refrigeration," Nat. Photonics **1**(12), 693–699 (2007).

[11] McCumber, D. E., "Einstein relations connecting broadband emission and absorption spectra," Phys. Rev. **136**(4A), 16–19 (1964).

[12] Melgaard, S. D., "Cryogenic optical refrigeration: Laser cooling of solids below 123 K," Diss. Univ. New Mex. (2013).

[13] Cittadino, G., Volpi, A. and Lieto, D., "Czochralski crystal growth for laser cooling," Opt. Eng. **56**(1), 1–15 (2018).

[14] Herriott, D. R. and Schulte, H. J., "Folded Optical Delay Lines," Appl. Opt. **4**(8), 883 (1965).

[15] Furukawa, G. T., Douglas, B., Mccoskeyr, R. E. and Ginnings, D. C., "Thermal Properties of Aluminum Oxide From 0-1200K," J. Res. Natl. Bur. Stand. (1934). **57**(2) (1956).

[16] Hehlen, M. P., Meng, J., Albrecht, R. A., Lee, E. R., Gragossian, A., Love, S. P., Hamilton, C. E., Epstein, R. I., and Sheik-Bahae, M., "First demonstration of an all-solid-state optical cryocooler" Light: Science & Applications accepted article preview 4 May 2018; doi: 10.1038/s41377-018-0028-7 (2018).